AIAA JOURNAL
Vol. 41, No. 8, August 2003

Hypervelocity Impacts on Thin Metallic and Composite Space Debris Bumper Shields

Djameel Ramjaun,* Ichiro Kato,† and Kazuyoshi Takayama‡
Tohoku University, Sendai 980-8577, Japan
and
Gopalan Jagadeesh§
Indian Institute of Science, Bangalore 560 012, India

The mechanism of hypervelocity impact crater formation in metallic and composite space debris shields has been investigated. Both normal and oblique impact crater formations have been investigated using 2.2-mm-thick aluminum (Al 2017), carbon fiber reinforced plastic (CFRP) and aramid fiber reinforced plastic (AFRP) space debris shields in a two-stage light gas gun. A cylindrical projectile made of high-density polyethylene (14 mm in diameter and length) at a muzzle speed of 5.0 ± 0.2 km/s is used to create the craters in the debris bumper shields. The microscopic study reveals the formation of adiabatic shear bands near the crater zone, from where the secondary cracks emerge, ultimately resulting in the formation of the craters in thin aluminium plates at impact angles of 90, 51, and 64 deg. On the other hand, surface delamination zones caused by the peeling of surface piles surrounding the impact and exit craters are observed in the case of CFRP and AFRP debris shields at normal impact. To estimate the temperature near the craters, time-integrated spectrum of the light emission during the crater formation is recorded. The measurements are taken in the near-UV region of the spectrum. Based on the CN emission from the projectile material, the temperature of the debris cloud during normal and oblique impacts at 5 km/s are estimated to be between 7300 ± 300 and 7600 ± 300 K, respectively.

I. Introduction

WITH the unrestrained proliferation of objects in outer space, the probability of space debris impact damaging a functional spacecraft is more likely now than ever before. In fact, space debris represents a significant hazard to the activities of the International Space Station project. Around 94% of the more than 7600 cataloged objects in orbit are categorized as debris.[1] However the actual number of debris objects in orbit far exceeds this cataloged population. The rapidly increasing probability of space debris colliding and damaging functional space vehicles and the distinct possibility of reentry of large space debris into inhabited areas and interfering with radio observations[2] are a real threat to space activities.

Many researchers[3–6] have investigated the material failure mechanism during high-velocity impact phenomenon with the ultimate goal of designing better shielding for spacecraft orbiting the Earth against space debris. Typically, space debris bumper shield design for long-duration spacecraft, as first proposed by Whipple,[7] consists of an outer bumper that is placed a small distance away from an inner wall or pressure wall of the spacecraft. The bumper protects by breaking up or vaporizing a debris particle such that the pressure wall is impacted by a relatively benign cloud of tiny particles instead of a single lethal particle. This type of bumper, as well as enhanced variations of it, such as the stuffed Whipple shields, have been investigated extensively for the last decade and proven to be effective in reducing the perforation threat of small high-speed projectiles. However, the recent higher risk of collision with large pieces of orbital debris has made necessary the modification of the design of bumper shields so that they can resist perforation by projectiles with much higher impact energies. In this respect, nonmetallic materials such as composite materials are now being used because they offer significant advantages over metals due to their high specific strength, high stiffness, and low coefficient of thermal expansion. However, the amount of experimental data compiled on the hypervelocity impact response of composite materials is quite scarce, and their potential use in the protection of spacecraft is still under evaluation. As for metallic bumpers, few microstructural analyses of craters formed on hypervelocity impacts can be found in the literature. For instance, Wingrove[6] evaluated the microstructure of craters formed in 10-mm-thick 2014 aluminum alloy targets impacted with steel projectiles of different shapes. However, the maximum velocity employed was only 240 m/s. In this paper, a summary of several experimental investigations of hypervelocity impacts of projectiles on metallic and nonmetallic materials is presented in which microstructural analyses of the craters have been made, as well as a spectroscopic study of the radiation emitted from the debris cloud.

Received 13 August 2002; revision received 15 April 2003; accepted for publication 15 April 2003.

*Japan Society for the Promotion of Science Research Fellow, Shock Wave Research Center, Institute of Fluid Science, 2-1-1, Katahira, Aoba-ku. Member AIAA.
†Graduate Student, Shock Wave Research Center, Institute of Fluid Science, 2-1-1, Katahira, Aoba-ku.
‡Director, Professor, Shock Wave Research Center, Institute of Fluid Science, 2-1-1, Katahira, Aoba-ku. Senior Member AIAA.
§Assistant Professor, Department of Aerospace Engineering. Member AIAA.

Hypervelocity Impact Process

The exact mechanism by which the impacting and target materials undergo fracture and ablation is a relatively complex process. Generally, it is agreed that, on impact, strong shock waves propagate along both the projectile and the target.[8] As the shock waves propagate, the projectile and bumper materials are heated adiabatically and nonisentropically. The release of the shock pressure occurs isentropically through the action of rarefaction waves that are created as the shock waves interact with projectile and bumper free surfaces (Fig. 1). This process leaves the projectile and bumper in high energy states, which can cause either or both to fragment, melt, or vaporize, depending on the material properties, geometric parameters, and velocity of impact.

If the impact velocity is sufficiently high, release from the impact shock results in a vaporized debris cloud, which is ejected from the sides at very high velocity. The material from this jet interacts with the surrounding gas, and because of its high velocity (usually several times the velocity of impact), undergoes further heating through localized shock waves. Eventually, as the temperature rises, a plasma

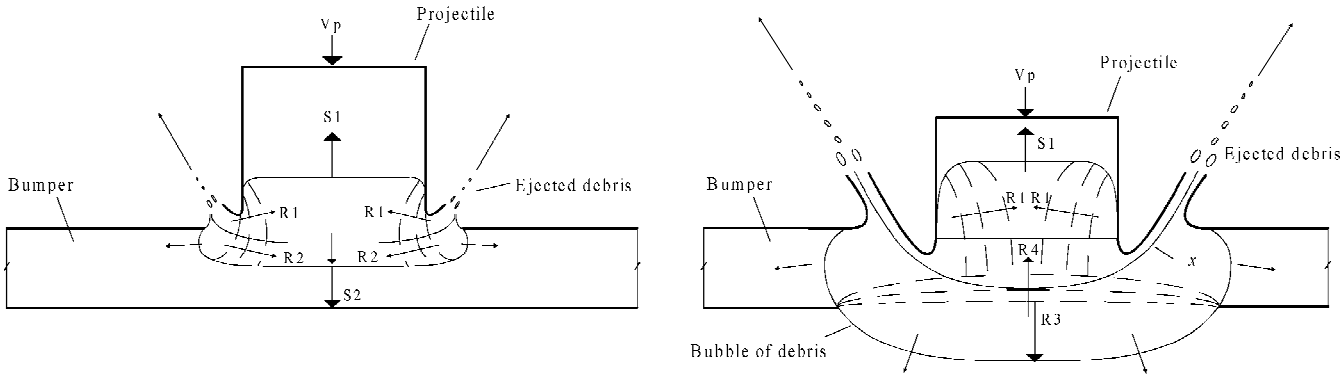

Fig. 1 Early stages of hypervelocity impact, from Anderson and Mullin.[8]

is formed in which several chemical dissociation reactions of the material involved occur. This plasma radiates strongly from the excitation and deexcitation processes undergone by its constituents. Therefore, it is expected that apart from blackbody radiation, strong line/band emissions will be observed from the debris cloud formed on the same side of the impact. On the opposite side of the bumper, a debris cloud is also formed consisting of fragments from both the projectile and target perforating through the bumper.

Synopsis of Experimental Investigation

Many issues, such as the appropriate material equation of state to be used in numerical simulations and the fracture mechanisms in hypervelocity impacts in composite materials under both normal and oblique impacts, still remain unclear. The complex state of material deformation during impact, followed by completely nonhomogenous material degradation is one of the unique features of hypervelocity impacts. In this backdrop, the objectives of the present study are as follows:

1) Study microscopically hypervelocity crater formation by the normal impact of the projectile at ~5 km/s on 2.2-mm-thick aluminum alloy (Al 2017), carbon fiber reinforced plastic (CFRP), and aramid fiber reinforced plastic (AFRP) space debris shields.

2) Do a high-speed visualization of the space debris during the crater formation process in Al 2017 shields at impact angles of 51, 64, and 90 deg.

3) Characterize the impact flash generated near space debris shields using emission spectroscopy in the near-UV region.

Moreover, very few studies address the problem of oblique impact on the space debris shields. Recent studies in the Shock Wave Research Center (SWRC) showed that the most probable oblique impact angle for the sidewall of a circular or square cylinder is around 53 deg, when random variable probability analysis is used. Based on this analysis, in the present study the hypervelocity crater formation process has been investigated at impact angles of 51 and 64 deg.

The energy partitioning mechanism by which the material is ejected and vaporized is not clear. Temperature measurements of the jetting vapor can, therefore, provide a better understanding of the physics of the impact vaporization. Early studies by Jean and Rollins[9] have confirmed that the radiation emitted from the fast jetting of debris from the front side consists mainly of atomic and molecular emission. This emission, if spectrally resolved, can provide a lot of information about the nature of the impact: material involved, correlation of flash intensity with velocity, and angle of impact. Thorough analysis of these spectra can even lead to the temperature reigning in this region. The spectroscopic study of the impact flash can be very useful in understanding the impact phenomenon. In the past, very few such studies have been done to analyze the jetting cloud. Recently, Sugita and Shultz[10,11] measured the emission lines of copper and calcium during impacts of quartz and copper projectiles on dolomite. Comparison of the experimental spectra with calculated ones yielded temperature estimations of the impact vapors formed in these experiments.

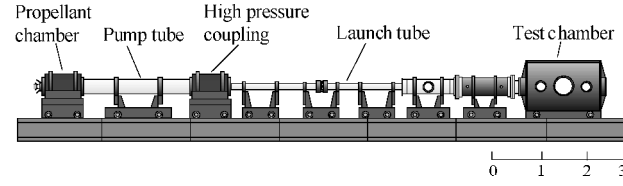

Fig. 2 Recently renovated two-stage light gas gun.

Tohoku University Ballistic Range

The ballistic range at the SWRC has been used routinely to test bumpers and other debris shielding materials, which will be used in the Japanese experimental module program.[12] The facility has been exhaustively used to study the flowfield around projectiles in the intermediate hypersonic regime[13,14] and also to visualize the debris produced by the normal impact of projectiles on both metallic and composite shields. To carry out the emission spectroscopic studies, the ballistic range was recently renovated by replacing the test section with optical quality quartz windows. A schematic diagram of the ballistic range is shown in Fig. 2. The total length of the ballistic range is 12 m comprising a 3-m-long pump tube of 60-mm internal diameter and a 4-m-long launch tube. Depending on the required projectile velocity to be simulated, two different launch tubes, 14 or 30 mm internal diameter, can be used. For technical reasons, all of the experiments in the present study are carried out by launching a 14-mm-diam, 1.5-g high-density polyethylene cylinder at muzzle speed of around 5 km/s. The free-flight section length is 5 m, and the nominal initial pressure in test air is maintained at about 600 Pa.

In the present experiments 2.2-mm-thick plates of Al 2017, CFRP, and AFRP are subjected to normal impact. The shields are removed after the shot, and the region near the crater is inspected under optical microscope and scanning electron microscope and subjected to microhardness tests. Oblique impact tests at impact angels of 51 and 64 deg to the axis of the ballistic range are also carried out using Al 2017 plates.

II. Investigation of Impact Craters

Al 2017 Bumper Shields

Small samples, covering a portion of the crater, were cut from the target plate for hardness measurements and for observations under a scanning electron microscope (SEM) and an optical microscope after the impact experiments. Surfaces of the samples (surface in the thickness direction as well as in the radial direction) were metallographically polished with a series of emery papers and diamond paste to a 0.5-μm surface finish. The Al 2017 sample was etched with Keller's reagent [2-ml HF (48%), 3-ml HCl (concentrate), 5-ml HNO_3 (concentrate), and 190-ml water] at 303 K for 10 s to reveal the grain structure.

Hardness measurements were carried out on the polished samples at regular intervals across the thickness, as well as in the radial direction starting from the crater wall, using a Vickers hardness tester

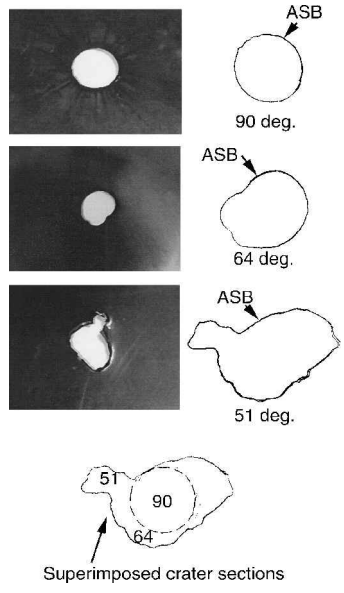

Fig. 3 Hypervelocity craters formed on a 2.2-mm-thick Al 2017 plate subjected to normal/oblique impact at 5 km/s.

(Tokyo Testing Equipments; Model Torsee) employing a 1-kg load. The wall of the crater surface of the samples was observed under SEM to investigate the mode of deformation.

Macroscopic Inspection

Figure 3 shows the superimposed contours of the craters formed on the Al 2017 plate at impact angles of 90, 64, and 51 deg. The normal impact produced a circular crater, whereas the crater shape is elongated at 64- and 51-deg impacts with increasing order. However, all of the three contours have a common region where similar microstructural features were observed. The contours with circular segments showed craters at the entry side and spalling at the rear side, whereas the elongated contours generally showed craters at the entry side and lip formation at the rear side indicating plastic deformation.

Microstructural Aspects

Normal impact (impact angle of 90 deg). Figure 4a shows the cross section of the damage caused by 90-deg impact. The arrow in the Fig. 4a indicates the direction of the projectile motion. The crater formed on the entry side and the spallations at the rear side

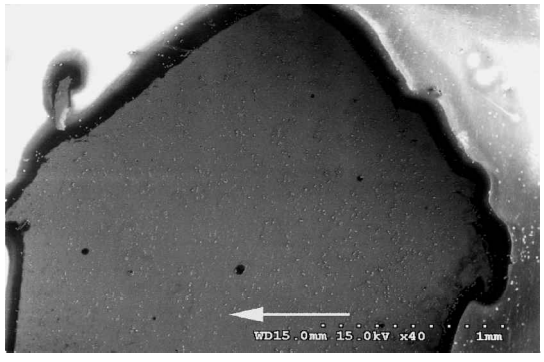

a)

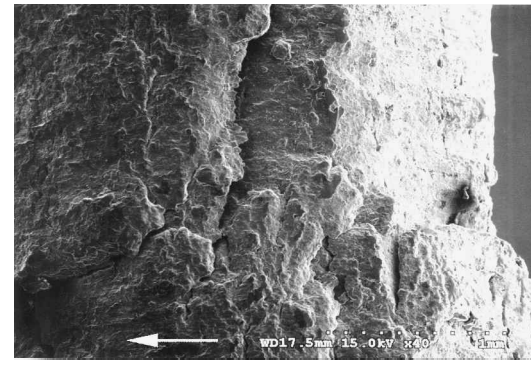

c)

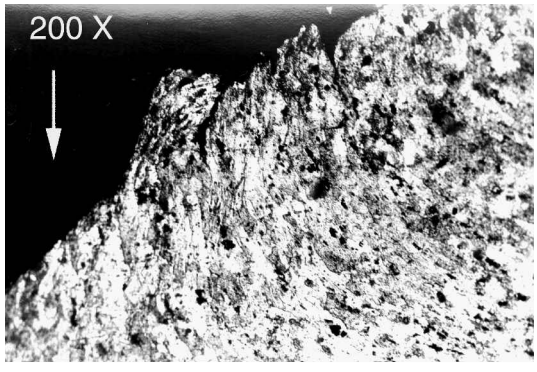

b)

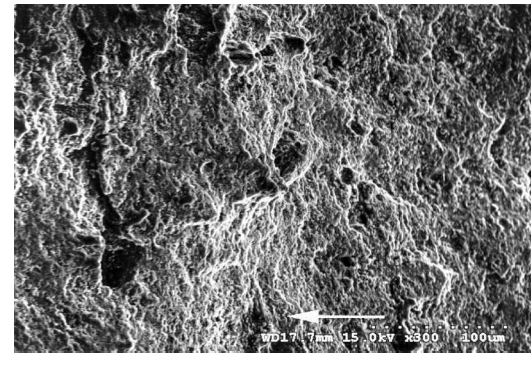

d)

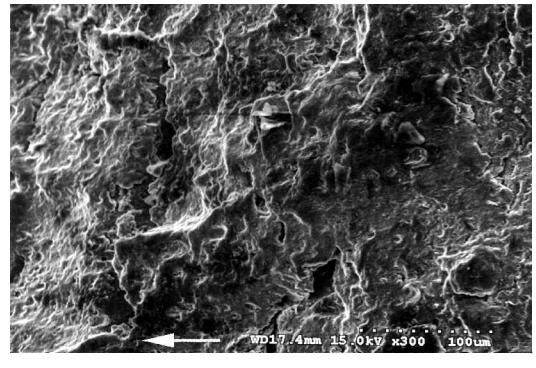

e)

Fig. 4 Microstructural observation of crater formed on the 2.2-mm-thick Al 2017 plate; impact angle equal to 90 deg and projectile velocity equal to 5 km/s.

are of similar shape and size. Figure 4b shows the microstructure of the crater cross section. The rim of the crater shows tear ridges, which indicate plastic ejection of material during impact, whereas the deeper part of the crater has been formed by secondary cracking because of adiabatic shear bands. Figure 4c shows the typical SEM image of the damage. The depth of the initial impact crater is approximately one-third of the total thickness, and the appearance of remaining damage is due to cracking of the material. Figures 4d and 4e show the SEM image of the crater surface, and spalled surface, respectively. Microcraters and cavitation due to ejection of particles could be observed on the entry side crater surface. The spalled region shows secondary cracking and cleavage surface, which is an indication of lower energy for fracture.

Vickers hardness results along the damage wall showed marginal increase of hardness on the plastically deformed regions. At the sites of intense plastic deformation, the measured hardness is between 126 and 130 kg/mm^2, whereas the hardness of Al 2017 plate before testing was around 120 kg/mm^2.

Oblique impact (64-deg impact angle). Figure 5a shows the cross section of the circular segment of the damage. The crater shape is found to be almost similar to that of 90-deg impact. The diamond-shaped black dots are indentations made during Vickers hardness measurement. A secondary crack running deep across the thickness from the rear side is observed. This cracking is due to formation of adiabatic shear bands and subsequent localized melting. The work done during intense plastic deformation due to hypervelocity impact causes a sharp rise in the local temperature. Projectile velocity, shape, and shock wave patterns determine the stress–strain condition of the target. The intersection of the shock waves develops high tensile stress. When localized melting occurs, even low tensile stress could result in cracking, as shown in Fig. 5b.

Figure 5c shows the cross section of the noncircular segment of the specimen damage. The crater also had a step and a deep secondary fracture. The rear side has spalled showing multiple secondary cracks. No symmetry between the entry and exit sides could be noticed, in contrast with 90-deg impact damage. Figure 5d shows the SEM image of the spalled surface. The stepped cleavagelike feature indicates that the crack has propagated preferentially through a particular crystallographic plane. It is not known whether these planes are usual {111} planes or low-density {100} planes showing low fracture energy. From the appearance, it is likely that these are low-density planes.

The Vickers hardness was measured along the crater wall cross section and near the secondary cracks. Even though the material along the cracking path, as well, as near the crater walls, visually exhibited heavy deformation, its hardness did not increase significantly. The difference in hardness between as-received and damaged material was of the order of 10 kg/mm^2. This could be attributed to the overaging of the plastically deformed material caused by internal temperature rise in opposition to the peak aged condition of the Al 2017 material used in the impact tests.

Oblique impact (51-deg impact angle). Figure 6a shows the cross section of the damage with circular segments. The features are similar to that of 64-deg impact. A number of secondary cracks could be observed emanating from the adiabatic shear bands. Generally, past observations have shown that crossing of radially developed cracks due to the lateral rarefaction waves, with the cracks due to shock waves, results in material spalling. Figure 6b shows the magnified SEM image of the elongated crack. As discussed earlier, in this case localized melting at the adiabatic shear band also resulted in cracking. Figure 6c shows the SEM image of the spalled region. A relatively flat and resolidified surface with secondary cracks could be observed. Figure 6d shows the cross section of the bulged region, where the damage due to plastic deformation occurred. No secondary cracks or spallation could be observed.

Hardness measurements were carried out across the spalled section, as well as the bulged segment. The secondary crack tip showed a hardness of 138 kg/mm^2. In the bulged region, the hardness slightly increased from the entry side (125 kg/mm^2) to exit side (135 kg/mm^2) but drastically decreased to 95 kg/mm^2 at a distance 0.3 mm from the rear side. The reason for this decrease in hardness is not clearly known. This behavior could be attributed to formation of microcavities.

Composite Bumper Shields

One of the characteristics of the impact on composite material is the surface delamination zone caused by the peeling of surface piles

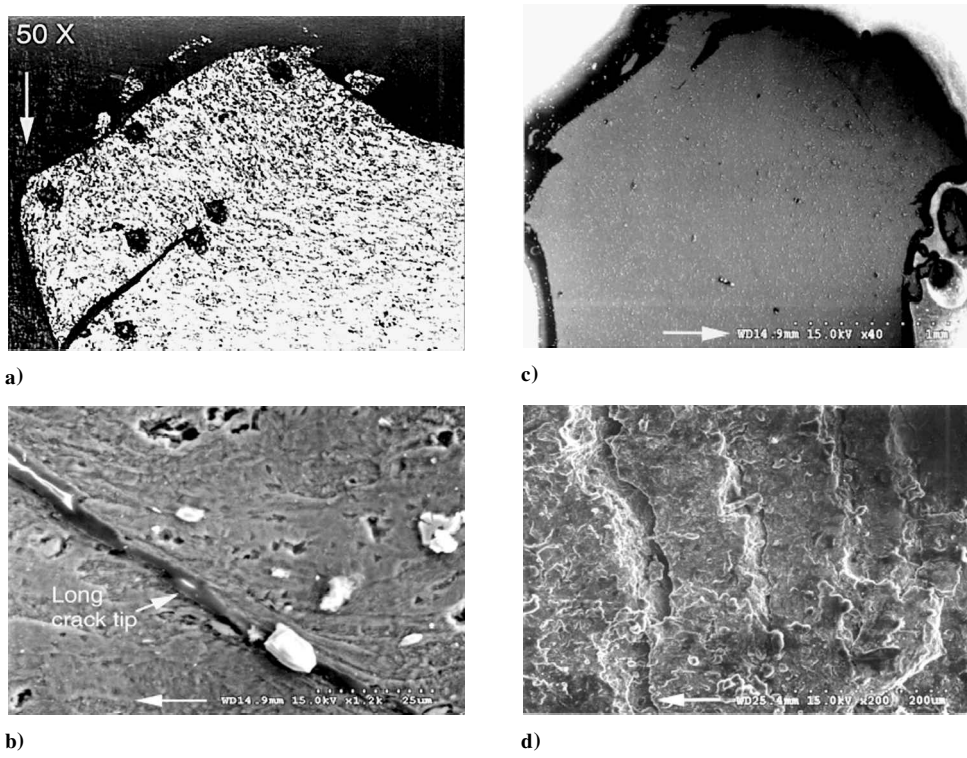

Fig. 5 Microstructural observation of crater formed on the 2.2-mm-thick Al 2017 plate; impact angle equal to 64 deg and projectile velocity equal to 5 km/s.

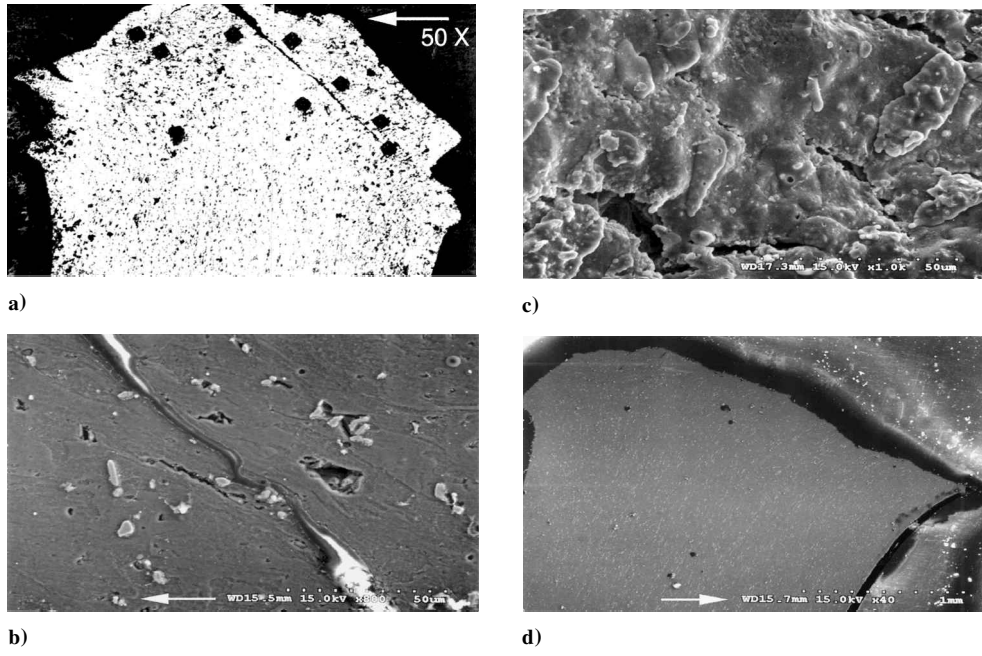

Fig. 6 Micro structural observation of crater formed on the 2.2-mm-thick Al 2017 plate; impact angle equal to 51 deg and projectile velocity equal to 5 km/s.

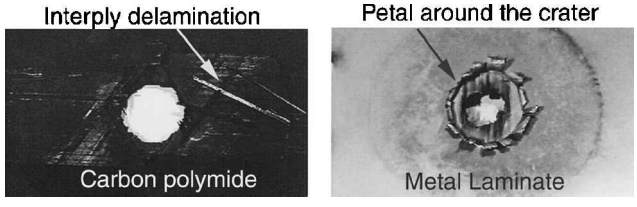

Fig. 7 Crater formed on the composite space debris shields; impact angle equal to 90 deg and projectile velocity equal to 5 km/s.

surrounding the impact and exit craters. This feature is clearly seen in Fig. 7 and confirms observations made in previous experiments.[15] This kind of damage is attributed to the reflection of the stress waves from the front and back free surfaces. Because these waves are propagating through layers of the material and not in a homogeneous medium, further tensile forces between the piles are created, leading to interply delamination and spall. The surface delamination in composites creates a larger damage zone, stripping off the protective coating along the surface ply, whereas the damage caused in metallic shields is restricted mainly to the impact crater. The vulnerability of a composite material to delamination results from the directional nature of its strength properties. Because the tensile wave propagates throughout the material, it can exceed the material strength in the direction where it is weakest. The strength properties of a metal, such as aluminum, are virtually isotropic, rendering it less vulnerable to rear surface damage and spallation. In this sense, the use of composite material as the outer bumper in multiwall bumper shields may be less effective than metals, which tend to spread the perforating debris cloud over a larger surface when impacted by a high-speed projectile. Because of delamination of the layers of the composite materials, it is not possible to examine the craters using scanning electron microscopy.

Discussion

Mechanism of Target Damage in Hypervelocity Impacts

Shear instabilities occur at various sites along the projectile/target interface under the high shear stresses and strain rates that arise as the projectile begins to penetrate the aluminum target. The local plastic work is converted into heat, and bands of concentrated shear displacements nucleate from these sites and grow into thermally softened aluminum.

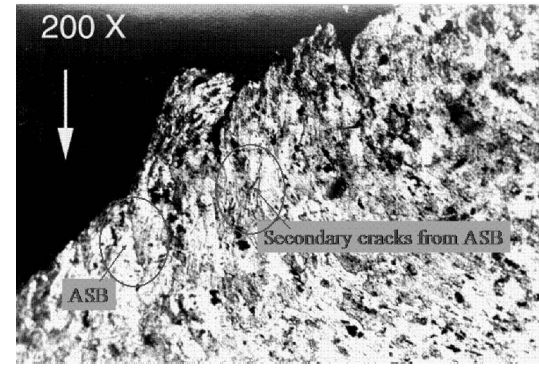

Fig. 8 ASBs near the crater in Al 2017 bumper plate; impact velocity equal to 5 km/s.

The generation of tensile stresses when the rarefaction waves intersect the free frontal surface of the target seems to be mainly responsible for the cracking in the shear bands and further nucleation and growth of the ductile fracture. This feature is predominantly observed at shear band intersections in the shock-heated material immediately beneath the crater. The preferential cracking along the shear bands can be attributed to the hard brittle nature and the residual stresses arising from the intense deformation and transformation. As shear band cracks link up with one another, they isolate chunks of aluminum from the front surface, thereby defining the final crater dimensions.

Adiabatic Shear Bands

The adiabatic shear bands (ASB) observed in the Al 2017 bumper shields near the crater is shown in Fig. 8. In fact, experiments were repeated using Al 2024 bumper shields at slightly lower projectile velocity (~4 km/s) to find out whether similar shear bands are observed at lower impact velocities. However, note that material compositions of Al 2024 and Al 2017 are almost similar and that even in the case of Al 2024 we observed the formation of ASB as seen in Fig. 9. Voids have also been observed within the shear bands resulting in selective formation of microvoids. It appears these voids grow under the influence of hydrostatic tension or negative pressure. There appears to be two mechanisms contributing to spall pressure increase within shear bands. First, the spall pressure is increased by

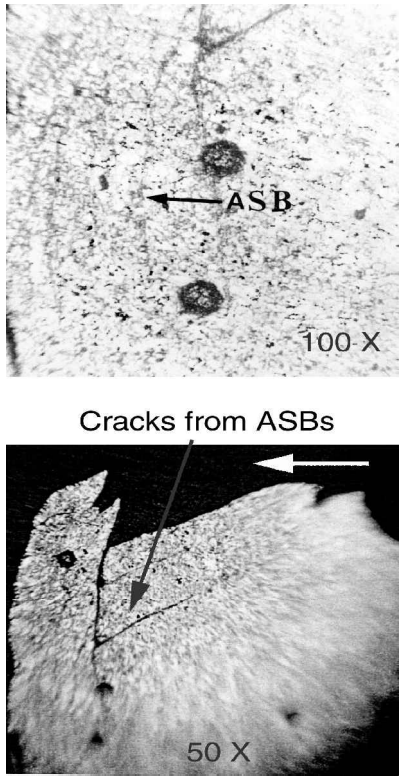

Fig. 9 ASBs near the crater in Al 2024 bumper plate; impact velocity equal to 4 km/s and normal impact.

any void nucleation and growth that occurred during the shear band formation. Second, thermal softening lowers the resistance to void growth, thereby, increasing the spall pressure.

The temperature rise due to adiabatic heating can be roughly expressed as

$$\frac{\mathrm{d}T}{\mathrm{d}t} = \left(\frac{\sigma}{C_v \rho}\right)\left(\frac{d\varepsilon}{\mathrm{d}t}\right) \tag{1}$$

where $\mathrm{d}T$ is temperature rise, σ tensile strength of the target, $\mathrm{d}\varepsilon/\mathrm{d}t$ strain rate, ρ density, and C_v specific heat. In this study, normal impact loading the aluminum alloy at 5-km/s velocity resulted in damage by crater formation at the entry side and spallation at the rear side. The crater was found to be enlarged by cracking due to shock wave interaction. Impacting at 64 deg also resulted predominantly in spallation. The reason for spallation was the intersection of shock wave and rarefaction waves at the ASBs wherein localized melting knocked off the bottom of the crater. In the case of 51-deg impact, the damaged area was enlarged. This expended additional energy could be a reason for decreased damage due to spallation.

Because the predominant mechanism of damage during high-velocity impact loading was found to be the formation of ASBs even in the case of thin plates of aluminum alloys, it is clear that materials that have no tendency to form adiabatic shears will have better resistance to impact loading. To achieve this, the material should have uniform and homogeneous flow properties during plastic deformation. Moreover, it should have higher melting point to prevent cracking in case of adiabatic shear formation. The material should not transform into a brittle phase during shock loading. Apart from these metallurgical parameters, ease of fabrication and low weight-to-strengthratio are other engineering constraints. Considering these factors, the possible candidate materials for future investigation for high-velocity impact barrier application could be pure aluminum, pure titanium, and Ni–Ti shape-memory alloys.

III. Emission Spectroscopy and High-Speed Visualization of Debris Cloud

Emission spectroscopy measurements are carried out to characterize the impact flash emitted around the debris shields. The ablation

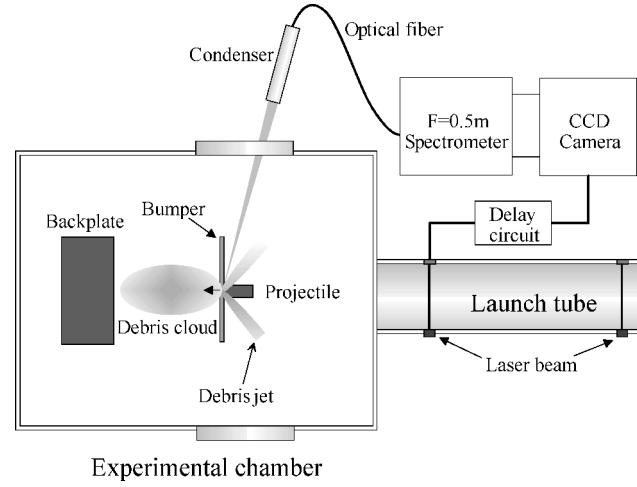

Fig. 10 Optical setup for emission spectroscopy of frontal debris cloud during hypervelocity impacts.

of high-density polyethylene projectile should result in significant amounts of emission from the CN radical. Simultaneously, in the initial stage of crater formation, the hypervelocity jetting of molten aluminum ejection further enhances the temperature around the crater. Hence, in the emission spectra, one would anticipate strong emissions from the ablated polyethylene projectile and also from the aluminum jet from the space debris bumper shield. The spectroscopic measurements are discussed in this section.

Experimental Setup

Figure 10 shows the emission radiated briefly on impact that is captured by a condenser lens placed at an angle of 15 deg and is guided by an optical fiber into a spectroscopic system and charge-coupled device (CCD) camera. The radiation is collected in a solid angle of about 0.008 sr around the region of impact. It is time integrated, that is, the recording of the CCD camera is triggered when the projectile cuts the laser beam situated in the free-flight section and stops about 30 μs after impact. Hence, the bulk of the radiation emitted during the impact event is captured by the system. For acquiring time-resolved spectra, a Hamamatsu Photonics streak unit was added to the setup at the output of the spectrometer. Time-resolved spectra in the form of 1024×256 images can thus be recorded by the CCD camera. The duration of the recording in the streak configuration was fixed to 50 μs, and the delay was adjusted to record 30–40 μs after the projectile impacts the plate. Two different test gases were used in the normal impact tests, dry air and N_2, at an average pressure of 600 and 2000 Pa. Magnesium projectiles have also been tested in N_2 and argon. However, because only impacts of polyethylene projectiles in N_2 gas are of quantitative interest, only the results from these experiments are presented. Indeed, aluminum reacts violently with oxygen, and because it is an exothermic reaction, the temperature in the impact zone artificially increases.

Temperature Determination

To deduce the temperature of the impact flash, the $\Delta v = 0$ emission band belonging to $B^2\Sigma^+ \leftrightarrow X^2\Sigma^+$ electronic transition of the CN radical was numerically simulated by using a spectroscopy application program called SPRADIAN.[16] This program calculates the emission spectra of several molecular species in a given medium according to a number of user-input data, such as the local thermodynamic parameters. It is expected that the temperature inferred from the CN spectrum will provide an estimate of the temperature around the impact point, in the surrounding jetting cloud. Several assumptions have to be made in the calculation of the spectrum and in its comparison to the experimental data:

1) The impact is taken as an equilibrium process. In the present case where temperature is determined from the time-integrated experimental radiation, it is expected that this value of temperature will be closer to the maximum attained in the gas near the impact

region. Also, a single temperature is considered, the vibrational and rotational temperatures being assumed to be the same.

2) Overlapping from other emission bands of N_2 and N_2^+ are ignored. This can be safely done because the contribution due to CN is very large compared to other species.

3) Line broadening due to pressure is taken into account in the calculation.

The relative intensities of the vibrational peaks of the $\Delta v = 0$ band of CN are very sensitive to temperature. The method of determination of the temperature from the measured spectra makes use of this characteristic by matching these peaks with values extracted from the calculated spectra. Only the first four vibrational levels are considered in this technique because the mutual overlapping of the higher levels makes the convergence of the calculation more difficult, and they are superfluous.

Experimental Results

Figure 11 shows an example of the emission spectrum of the impact flash measured during a normal impact on aluminum. Tests using magnesium projectiles on aluminum bumpers yielded no CN bands, thus, confirming that these bands do not originate from contamination of the experimental chamber. Strong emission of the 394.4- and 396.2-nm Al lines, as well as some magnesium lines when using projectiles of this metal, could also be detected.

Figure 12 shows the sequential images as captured by an image converter camera during a normal impact. The flashes correspond to two distinctively separated phenomena, which were also observed by Jean and Rollins.[9] The first shorter-duration flash, as shown by frames 2 and 3, lasting for less than 10 μs, corresponds to atomic radiation from shock-heated material near to the impact zone and the second, frames 6–8, to molecular radiation as the debris cloud interacts with the surrounding gas. Spectroscopic verification of these emissions was done by time-resolved spectroscopy, using a streak unit, and is shown in Fig. 13a. Because of the technical limitations of the present streak setup, this measurement was done only in very low spectral resolution. Time evolutions of the emission from Al and CN/N_2^+ bands could be distinguished and are, thus, plotted in Fig. 13b. Within the present temporal resolution of the system, which is of the order of 1 μs the onset of these bands coincides with the corresponding emission on the sequential photographic results. That is, line emission from aluminum is emitted as soon as it is being heated on impact and vaporized in the debris jet. Probably, the aluminum vapor cools down as it expands in the surrounding gas, which explains the brief nature of its emission. Debris from the polyethylene projectile vaporizes very quickly, but takes a longer time to be heated in the surrounding gas through localized shock waves. Eventually, the material undergoes successive dissociation and recombination reactions, which lead to formation of radicals such as CN and N_2^+, responsible for the strong band emissions observed in Fig. 13b, lasting for more than 20 μs. It is essentially the second flash that is being measured and analyzed by spectroscopy in the present study.

When the method described in the preceding section is used, the average temperatures of the different impact tests are calculated (example in Fig. 14) and summarized in Fig. 15. The error bars are determined from the uncertainty in matching the experimental spectrum data with calculation. In the case of oblique angle impacts,

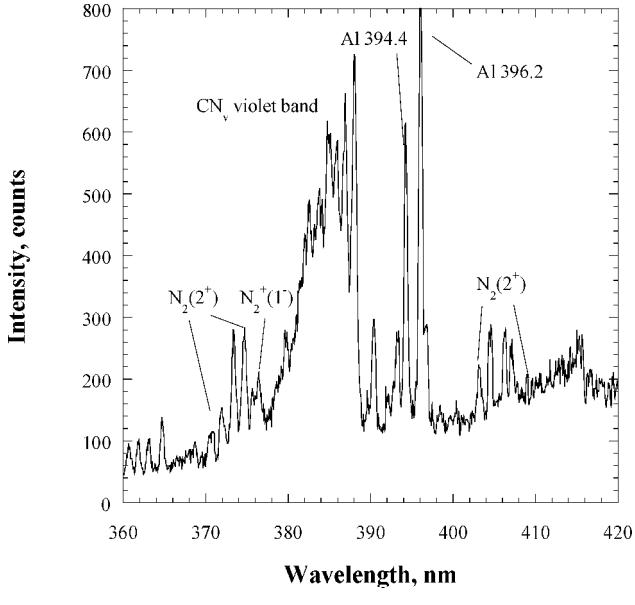

Fig. 11 Time-integrated spectroscopy of debris cloud during normal impact of polyethylene projectile on aluminum bumper; projectile velocity equal to 5.1 km/s in N_2 gas at 600 Pa.

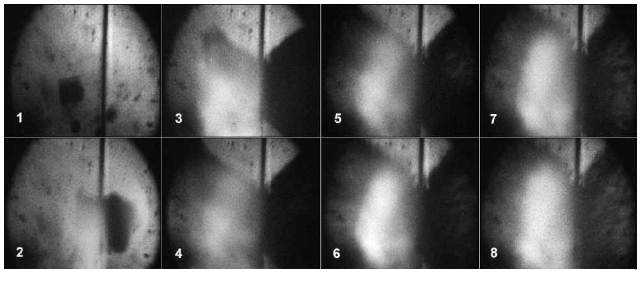

Fig. 12 Image converter camera visualization of normal impact on Al bumper, projectile velocity equal to 5 km/s in N_2 gas at 600 Pa; interframe equal to 8 μs and exposure equal to 15 ns.

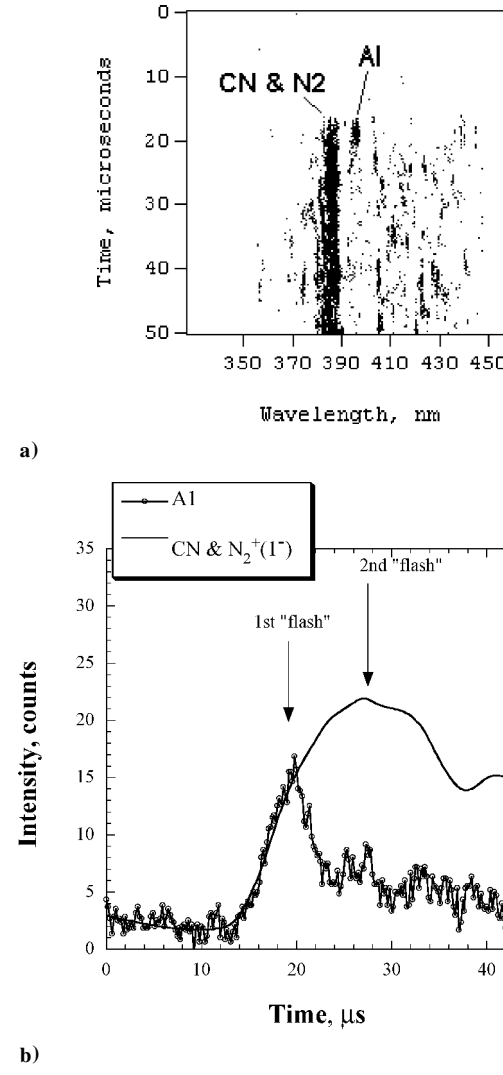

Fig. 13 Time-resolved spectroscopy, normal impact on Al; projectile velocity equal to 5 km/s in N_2 at 600 Pa.

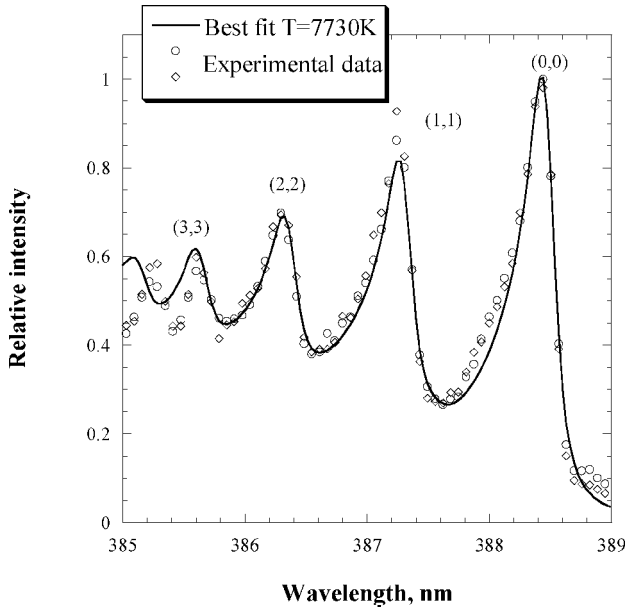

Fig. 14 Best fit of $\Delta v = 0$ emission band of CN spectrum yields $T = 7730 \pm 460$ K for oblique impacts on Al; projectile velocity equal to 5 km/s in N_2 at 600 Pa.

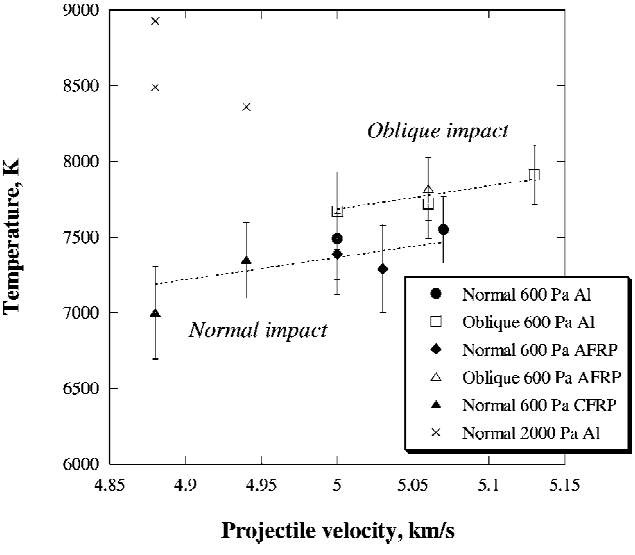

Fig. 15 Summary of estimated impact temperature of debris cloud in different experimental conditions.

because no clear distinction could be made between the two different angles tested, data from these two sets are analyzed together. The mean value of the temperature during normal impacts of polyethylene projectiles on an aluminum bumper in N_2 gas under the present experimental conditions is estimated to be slightly lower than in oblique conditions, about 300 K for impacts at 5 km/s. This discrepancy seems to be larger in the case of impacts on AFRP, where the temperature difference between normal and oblique impacts is of the order of 500 K. For CFRP, this trend could not be verified. However, note that the different tendencies exhibited by the estimated debris cloud temperatures are within the experimental error range. Therefore, before confirming these tendencies, more experiments are mandatory.

Discussion on Debris Cloud Spectroscopy

The formation of the debris cloud is clearly a complex phenomenon, and the temperatures derived in this paper from the emission of CN depend on many successive chemical dissociation and recombination steps. Moreover, the debris cloud as observed here has experienced substantial adiabatic decompression after jetting out of the impact point. The correlation between the temperatures deduced in the present work with the velocity of impact, and as well as with the angle of impact, is consistent with past observations.[10,11] However, these temperatures are based on molecular emission, and a closer estimate of the temperature of the impact would be expected if it were deduced from observation of atomic lines emission. Indeed, molecular emission arises from the secondary interaction of the debris with the surrounding gas. Therefore, in this case it is difficult to trace back the initial conditions of the debris jet precisely, which have already undergone a number of chemical reactions. Experimentally, this would explain that temperatures deduced for impacts on different target materials were of the same order, except for tests that bore clearly different conditions, such as angle of impact and ambient gaseous pressure. Analysis of line emission from atomic excitation leads directly to the intended impact conditions. However, its accuracy depends on the availability of an emitter exhibiting a large number of emission lines, as widely distributed in energy levels as possible. Copper fits in well in this category and could be used in the projectile in future investigations.

For tests done at higher pressure, it is found that the temperature of the debris cloud is sensibly higher, which is intuitively expected. Note also that previous tests done in air instead of nitrogen yielded much higher temperatures because the presence of O_2 favored some exothermic reactions in the cloud. For this reason, nitrogen is preferred as test gas because it provides a more neutral environment for the debris cloud to develop.

Note that the method of measuring integrated emission, as used here, tends to give the highest temperature attained during the impact process. Certainly, the in-depth differences between the normal and oblique impact processes cannot be captured by the time-integrated measurements. An accurate time-resolved analysis of the process by acquisition of time-resolved spectroscopy would have given valuable information on the formation of the jetting cloud in the oblique impacts, but unfortunately, the present time-resolving capacity of the system in the streak configuration is severely limited. However, these preliminary time-resolved spectroscopy results yielded interesting details on the impacts in different experimental conditions.

IV. Conclusions

Crater formation in both metallic and nonmetallic space debris bumper shields in hypervelocity impacts has been investigated. The study reveals the formation of ASBs near the crater as a possible mechanism of hypervelocity spallation in Al 2017 debris shields at impact angles of 90, 51, and 64 deg. This suggests that materials that have uniform and homogeneous flow properties during plastic deformation will have better resistance to impact loading. Tests on composite bumper shields have confirmed that, during impacts, surface delamination causes the peeling of surface piles surrounding the impact and exit craters, thus, creating a large damage zone. Therefore, composites do not necessarily provide an advantage over metallic bumpers, and suggestions to their use more as inner bumpers than outer bumpers may be justified. The emission spectrum of the CN violet has been measured, and analysis of it, by comparison to calculation, has yielded average temperatures of the jetting cloud in different experimental conditions. In general, tests in normal impact gave lower temperatures than in oblique impact, suggesting a higher energy state of the debris cloud in the latter case. No clear distinction could be made between the debris cloud temperatures deduced from impacts on different target materials because of the nature of the technique itself. To get more accurate estimates of the temperature of the impact zone, future calculations should be based on metallic line emission spectra. For this purpose, copper is more suitable as projectile material than polyethylene or aluminum. Time-resolved spectroscopy and high-speed sequential visualization have also been carried out. Results obtained have revealed that line/metallic emission occurs briefly around the impact zone and molecular emission, for a longer duration of time, in the expanding debris cloud. Recently, the laboratory has acquired a new high-performance two-stage light gas gun, and preliminary tuning of the facility is under way. This gun will enable the study of hypervelocity impacts at higher velocities (8 km/s or above).

References

[1]Barrows, S. P., Swinerd, C. G., and Crowther, R., "Review of Debris-Cloud Modeling Techniques," *Journal of Spacecraft and Rockets*, Vol. 33, No. 4, 1996, pp. 550–555.

[2]Ganeshan, A. S., "Modeling the Low Earth Space Debris Environment," *Journal of Spacecraft Technology*, Vol. 4, No. 2, 1994, pp. 52–59.

[3]Shocky, D. A, Curran, D. R., and De Carli, P. S., "Damage in Steel Plates from Hypervelocity Impact. I. Physical Changes and Effect of Projectile Material," *Journal of Applied Physics*, Vol. 46, No 9, 1975, pp. 3766–3775.

[4]Zhou, J. S., Zhen, L., Yang, D. Z., and Li, H. T., "Macro and Micro Damage Behaviors of the 30CrMnSiA Steel Impacted by Hypervelocity Projectiles," *Material Science and Engineering*, Vol. A282, pp. 177–182.

[5]Zhou, J. S., Zhen, L., Cui, Y. X., and Zhang, D. Z., "Transformed Shearing Bands in Strongly Impact Loaded 30CrMnSiA Steel," *Journal of Materials Science Letters*, Vol. 17, 1998, pp. 391–393.

[6]Wingrove, A. L., "The Influence of Projectile Geometry on Adiabatic Shear and Target Failure," *Metallurgical Transactions*, Vol. 4, 1973, pp. 1829–1833.

[7]Whipple, F. L., "Meteorites and Space Travel," *Astronomical Journal*, Vol. 52, 1947, p. 5.

[8]Anderson, C. E., and Mullin, S. A., "Hypervelocity Impact Phenomenology: Some Aspects of Debris Cloud Dynamics," *Proceedings of the First International Conference on Effects of Fast Transient Loadings*, edited by W. J. Ammann, W. K. Liu, J. A. Studer, and T. Zimmermann, Balkema, Rotterdam, The Netherlands, 1988, pp. 105–122.

[9]Jean, B., and Rollins, T. L., "Radiation from Hypervelocity Impact Generated Plasma," *AIAA Journal*, Vol. 8, No. 10, 1970, pp. 1742–1748.

[10]Sugita, S., and Schultz, P. H., "Spectroscopic Measurements of Vapor Clouds due to Oblique Impacts," *Journal of Geophysical Research*, Vol. 103, No. E8, 1998, pp. 19, 427–19, 441.

[11]Sugita, S., and Schultz, P. H., "Spectroscopic Characterization of Hypervelocity Jetting: Comparison with a Standard Theory," *Journal of Geophysical Research*, Vol. 104, No. E12, 1999, pp. 30, 825–30, 845.

[12]Nonaka, S., and Takayama, K., "Overview of Ballistic Range Program at Tohoku University," AIAA Paper 98-2604, June 1998.

[13]Nonaka, S., "Experimental and Numerical Study on Hypersonic Flows in Ballistic Range," Ph.D. Dissertation, Dept. of Aeronautics and Space Engineering, Tohoku Univ., Sendai, Japan, Jan. 2000.

[14]Nonaka, S., Mizuno, H., Hashimoto, T., and Takayama, K., "Density Measurements over a Sphere in Ballistic Range," AIAA Paper 2000-0837, Jan. 2000.

[15]Schonberg, W. P., "Protecting Spacecraft Against Orbital Debris Impact Damage Using Composite Materials," *Composites Part A: Applied Science and Manufacturing*, Vol. 31, No. 8, 2000, pp. 869–878.

[16]Fujita, K., and Abe, T., "SPRADIAN, Structured Package for Radiation Analysis: Theory and Application," Inst. of Space and Astronautical Science, ISAS Rept. 669, Kanagawa, Japan, Sept. 1997.

A. N. Palazotto
Associate Editor